Nano Research
2024, 17(7): 6734–6740

ISSN 1998-0124 CN 11-5974/O4
https://doi.org/10.1007/s12274-024-6609-2

Superatom-assembled boranes, carboranes, and low-dimensional boron nanomaterials based on aromatic icosahedral B_{12} and C_2B_{10}

Qiao-Qiao Yan, Yan-Fang Wei, Qiang Chen (✉), Yue-Wen Mu (✉), and Si-Dian Li (✉)

Institute of Molecular Science, Shanxi University, Taiyuan 030006, China

Received: 29 December 2023 / **Revised:** 18 February 2024 / **Accepted:** 29 February 2024

ABSTRACT

Using the experimentally known aromatic icosahedral superatoms I_h $B_{12}H_{12}^{2-}$ and D_{5d} 1,12-$C_2B_{10}H_{12}$ as building blocks and based on extensive density functional theory calculations, we predict herein a series of core–shell superpolyhedral boranes and carboranes in a bottom-up approach, including the high-symmetry T_h $B_{12}@B_{152}H_{72}^{2-}$ (**2**), C_{2h} $C_2B_{10}@B_{152}H_{72}$ (**3**), D_{3d} $B_{12}@B_{144}H_{66}$ (**4**), I_h $B_{12}@C_{24}B_{120}H_{72}^{2-}$ (**6**), and D_{5d} $C_2B_{10}@C_{24}B_{120}H_{72}$ (**7**). More interestingly, the superatom-assembled linear D_{2h} $B_{36}H_{32}^{2-}$ (**8**), close-packed planar D_{3d} $B_{84}H_{60}^{2-}$ (**10**), and nearly close-packed core−shell D_{3d} $B_{12}@B_{144}H_{66}$ (**4**) can be extended periodically to form the one-dimensional (1D) α-rhombohedral borane nanowire $B_{12}H_{10}$ (*Pmmm*) (**9**), two-dimensional (2D) α-rhombohedral monolayer borophane $B_{12}H_6$ ($P\bar{3}m1$) (**11**), and the experimentally known three-dimensional (3D) α-rhombohedral boron ($R\bar{3}m$) (**12**) which can be viewed as an assembly of the monolayer $B_{12}H_6$ (**11**) staggered in vertical direction, setting up a bottom-up strategy to form low-dimensional boron-based nanomaterials from their borane "seeds" via partial or complete dehydrogenations. Detailed bonding analyses indicate that the high stability of these nanostructures originates from the spherical aromaticity of their icosahedral B_{12} or C_2B_{10} structural units which possess the universal skeleton electronic configuration of $1S^21P^61D^{10}1F^8$ following the Wade's n+1 rule. The infrared (IR) and Raman spectra of the most-concerned neutral $B_{12}@B_{144}H_{66}$ (**4**) and $C_2B_{10}@C_{24}B_{120}H_{72}$ (**7**) are computationally simulated to facilitate their experimental characterizations.

KEYWORDS

superatom-assembling, bottom-up approach, density functional theory, superpolyhedral boranes, superpolyhedral carboranes, borophanes

1 Introduction

Increasing experimental and theoretical evidences in the past two decades suggest that cluster superatoms may serve as building blocks to form self-assembled compounds and nanomaterials in bottom-up approaches [1–4]. The best experimentally known superatoms in boron chemistry are the 12-vertex icosahedral borane I_h $B_{12}H_{12}^{2-}$ (^1A_g) and icosahedral carborane D_{5d} 1,12-$C_2B_{10}H_{12}$ ($^1A_{1g}$) due to their superb chemical stabilities [5–10]. Both these icosahedral species prove to follow the superatomic configuration of $1S^21P^61D^{10}1F^8$ (see Fig. S1 in the Electronic Supplementary Material (ESM)) and match the Wade's n+1 rule in skeleton-electron counts [11], making them spherically aromatic in nature. It is also well known that all the seventeen bulk boron allotropes experimentally observed to date contain icosahedral B_{12} structural units which, in most cases, are accompanied by certain numbers of boron atoms lying outside the cages as interstitial atoms [12, 13], except the simplest form, α-rhombohedral boron (α-B_{12}) firstly synthesized in 1958 [14], which contains a D_{3d} B_{12} icosahedral unit cell in a nearly close-packed arrangement. In fact, with six B–B 2c–2e σ bonds on the top and bottom and six B–B–B 3c–2e σ bonds on the waist, each D_{3d} B_{12} unit cell in α-B_{12} matches the Wade's n+1 rule as a spherically aromatic structural unit as discussed in details late, making α-B_{12} unique in boron bulk allotropes. Monolayer γ-B_{28} composed of icosahedral B_{12} clusters and B_2 dumbbells was synthesized in 2015 on copper foils by chemical vapor deposition at low pressures with hydrogen as carrier gases [15]. However, small bare $B_n^{-/0}$ clusters (n < 19) characterized in gas phases by persistent joint photoelectron spectroscopy (PES) and first-principles theory investigations in the past two decades all possess planar or quasi- planar structures, with their cage-like isomers with unsaturated dangling bands on the surfaces being much less stable in thermodynamics [16–22]. Neutral B_{12} as the bare boron cluster most-concerned in this work has been experimentally confirmed to have a quasi-planar C_{3v} structure analogous to benzene (C_6H_6) in π bonding [16, 20]. The smallest bare cage-like B_n cluster characterized in PES experiments is the seashell-like C_2 $B_{28}^{0/-}$ [23], followed by chiral cage-like C_3/C_2 B_{39}^- [24], cage-like D_{2d} $B_{40}^{-/0}$ [25], and bilayer D_{2h} $B_{48}^{-/0}$ [26]. Obviously, how to form bulk boron allotropes from bare B_n clusters or closo-icosahedral boranes in a bottom-up approach still remains unknown to date in both experiments and theory.

Keeping the inspiration in mind and based on icosahedral $B_{12}H_{12}^{2-}$ and 1,12-$C_2B_{10}H_{12}$, we predict in this work at density-functional theory (DFT) level a series of superatom-assembled core–shell superpolyhedral boranes and carboranes T_h $B_{12}@B_{152}H_{72}^{2-}$ (**2**), C_{2h} $C_2B_{10}@B_{152}H_{72}$ (**3**), D_{3d} $B_{12}@B_{144}H_{66}$ (**4**), I_h $B_{12}@C_{24}B_{120}H_{72}^{2-}$ (**6**), and D_{5d} $C_2B_{10}@C_{24}B_{120}H_{72}$ (**7**) in the structural motif of C_{60}. The linear D_{2h} $B_{36}H_{32}^{2-}$ (**8**), close-packed planar D_{3d} $B_{84}H_{60}^{2-}$ (**10**), and core–shell D_{3d} $B_{12}@B_{144}H_{66}$ (**4**)

Address correspondence to Qiang Chen, chenqiang@sxu.edu.cn; Yue-Wen Mu, ywmu@sxu.edu.cn; Si-Dian Li, lisidian@sxu.edu.cn

assembled in similar patterns have been extended to form the infinite one-dimensional (1D) α-rhombohedral borane nanowire $B_{12}H_{10}$ (*Pmmm*) (**9**), two-dimensional (2D) α-rhombohedral monolayer borophane $B_{12}H_6$ ($P\bar{3}m1$) (**11**), and three-dimensional (3D) α-rhombohedral boron ($R\bar{3}m$) (α-B_{12}) (**12**), presenting a bottom-up approach to form borane and carborane nanoclusters and their corresponding low-dimensional nanomaterials by superatom-assembling via partial or complete dehydrogenations.

2 Theoretical procedures

The manually constructed superatom-assembled superpolyhedral boranes and carboranes in the structural motifs of C_{60} via partial-dehydrogenizations were fully optimized at both the hybrid Perdew–Burke–Ernzerhof (PBE0)/6-31G(d) and B3LYP/6-31G(d) levels [27, 28] in Fig. 1, with both their vibrational frequencies and stabilities of wavefunctions checked to ensure that all obtained structures are true minima of the systems. The high-symmetry core–shell **2**, **3**, **4**, **6**, and **7** in Fig.1 and linear $B_{36}H_{32}{}^{2-}$ (**8**) and close-packed planar $B_{84}H_{60}{}^{2-}$ (**10**) in Fig. 2 appeared to be much more stable (at least 2.10 eV) than their distorted triplet and quintet counterparts at PBE0. As a demonstration, the perfect superpolyhedral borane I_h $C_{24}B_{120}H_{84}$ (**5**) (^1A_g) [29] was manually constructed by substituting the twelve C_5 pentagons on the surface of C_{60} with twelve D_{5d} 1,12-$C_2B_{10}H_{12}$ superatoms with the C_5 molecular axis located exactly perpendicular to the cage surface towards the cage center, leading to the formation of thirty inter-cage B–B σ bonds and release of thirty H_2 molecules. The perfect core–shell I_h $B_{12}@C_{24}B_{120}H_{72}{}^{2-}$ (**6**) (^1A_g) with an icosahedral B_{12} core covalently saturated by twelve inter-cage B–C σ bonds (~ 1.60 Å) was obtained by incorporating an I_h $B_{12}H_{12}{}^{2-}$ at the center of $C_{24}B_{120}H_{84}$ (**5**) to release 6 H_2 molecules, while the core–shell D_{5d} $C_2B_{10}@C_{24}B_{120}H_{72}$ (**7**) (^1A_g) with an icosahedral D_{5d} C_2B_{10} core was achieved by incorporating a D_{5d} C_2B_{10} core at the center of the $C_{24}B_{120}H_{84}$ (**5**) shell. Nucleus-independent chemical shifts (NICS) [30, 31] were calculated at the geometrical centers to check the spherical aromaticity of systems, with the corresponding NICS-ZZ distributions obtained using the Multiwfn 3.8 code [32]. The infrared (IR) and Raman spectra of neutral $B_{12}@B_{144}H_{66}$ (**4**) and $C_2B_{10}@C_{24}B_{120}H_{72}$ (**7**) were simulated at PBE0/6-31G(d).

Structural optimizations on 1D, 2D, and 3D crystals were carried out using the Vienna *ab initio* simulation package (VASP 5.4) [33, 34] at DFT level within the PBE parametrization of generalized gradient approximation (GGA) [35]. A vacuum slab (more than 15 Å) was selected to prevent mirror interactions and a plane-wave basis set with an energy cutoff of 500 eV was used. The Brillouin zones were sampled with 2π × 0.02 $Å^{-1}$ spacing in the reciprocal space by the Monkhorst–Pack scheme [36]. Atomic structures were fully relaxed using the conjugate gradient method until the maximum force on each atom was less than 10^{-3} eV·$Å^{-1}$ and the energy precision was set to 10^{-5} eV per atom. The phonon dispersion spectra of 1D $B_{12}H_{10}$ (**9**), 2D $B_{12}H_6$ (**11**), and 3D α-B_{12} (**12**) were calculated using the density-functional perturbation theory (DFPT) method implemented in the Phonopy program [37] interfaced with VASP, with their band structures obtained at the hybrid HSE06 level [38] (Fig. 3).

Born-oppenheimer molecular dynamics (BOMD) simulations were performed on the concerned species for 30 ps using the CP2K program [39], with the Goedecker–Teter–Hutter (GTH)-PBE pseudopotential and DZVP-MOLOPT-SR-GTH basis sets used for B, C, and H. Chemical bonding analyses were performed on isolated clusters using the adaptive natural density partitioning (AdNDP) approach [16, 40] and on 1D, 2D, and 3D crystals utilizing the solid-state AdNDP (SSAdNDP) [41]. The results were visualized using the VMD 1.9.3 program [42]. The calculations on zero-dimensional clusters were performed utilizing the Gaussian 16 software [43] and on low-dimensional crystals employing the VASP software.

3 Results and discussions

3.1 Structures and stability

The superatom-assembled high-symmetry superpolyhedral borane T_h $B_{152}H_{84}$ (**1**) and carborane I_h $C_{24}B_{120}H_{84}$ (**5**) and their core–shell superpolyhedral counterparts T_h $B_{12}@B_{152}H_{72}{}^{2-}$ (**2**), C_{2h} $C_2B_{10}@B_{152}H_{72}$ (**3**), D_{3d} $B_{12}@B_{144}H_{66}$ (**4**), I_h $B_{12}@C_{24}B_{120}H_{72}{}^{2-}$ (**6**), and D_{5d} $C_2B_{10}@C_{24}B_{120}H_{72}$ (**7**) optimized at both PBE0/6-31G(d) and B3LYP/6-31G(d) levels are collectively depicted in Fig. 1. With the valences of all the component surface atoms fully satisfied by either terminal -H atoms, bridging -H- atoms, or inter-cage B–B or B–C σ interactions on the cage surfaces, the obtained **1**–**7** with stable wavefunctions all turn out to be true minima of the systems without imaginary vibrational frequencies, as tabulated in Table 1. The suprapolyhedral boranes and carboranes with a closo-B_{12} or closo-C_2B_{10} core at the center possess the large highest occupied molecular orbital (HOMO)–lowest unoccupied molecular orbital (LUMO) gaps between E_{gap} = 2.85–7.09 eV

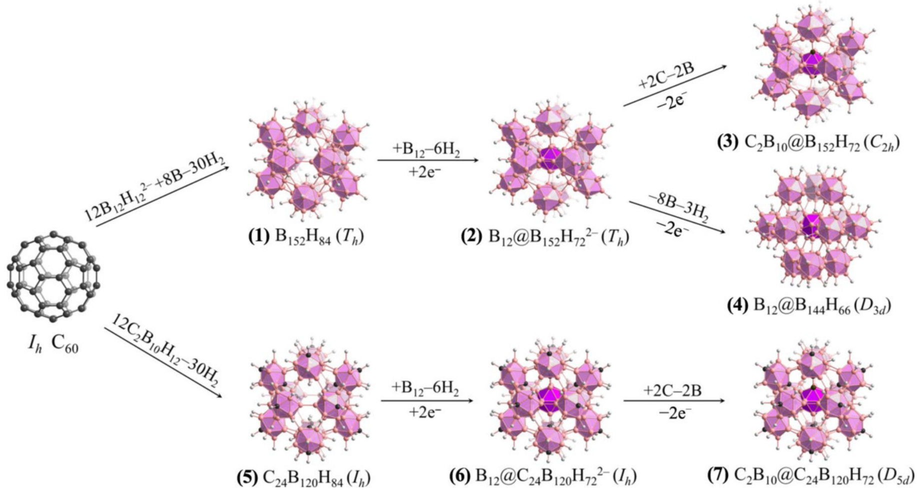

Figure 1 Optimized structurers of the superatom-assembled T_h $B_{152}H_{84}$ (**1**) and I_h $C_{24}B_{120}H_{84}$ (**5**) and their core–shell superpolyhedral counterparts T_h $B_{12}@B_{152}H_{72}{}^{2-}$ (**2**), C_{2h} $C_2B_{10}@B_{152}H_{72}$ (**3**), D_{3d} $B_{12}@B_{144}H_{66}$ (**4**), I_h $B_{12}@C_{24}B_{120}H_{72}{}^{2-}$ (**6**), and D_{5d} $C_2B_{10}@C_{24}B_{120}H_{72}$ (**7**) at PBE0/6-31G(d) and B3LYP/6-31G(d) levels using the icosahedral $B_{12}H_{12}{}^{2-}$ and 1,12-$C_2B_{10}H_{12}$ as building blocks in the structural motif of I_h C_{60} via partial dehydrogenations (pink B, black C, and white H, with the 12-vertex polyhedrons highlighted in purple).

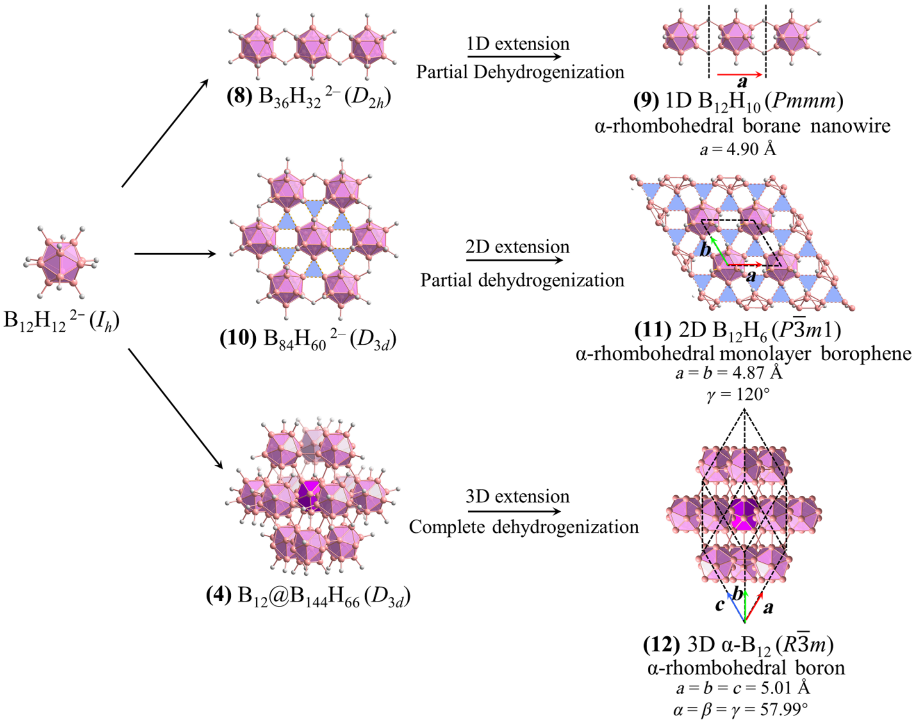

Figure 2 Optimized superatom-assembled linear D_{2h} $B_{36}H_{32}{}^{2-}$ (**8**), close-packed hexagonal D_{3d} $B_{84}H_{60}{}^{2-}$ (**10**), and nearly close-packed core–shell D_{3d} $B_{12}@B_{144}H_{66}$ (**4**) and their extended periodic nanomaterials 1D α-rhombohedral borane nanowire $B_{12}H_{10}$ ($Pmmm$) (**9**), 2D α-rhombohedral monolayer borophane $B_{12}H_6$ ($P\bar{3}m1$) (**11**), and 3D nearly close-packed α-rhombohedral boron ($R\bar{3}m$) (**12**) at GGA-PBE level, with the optimized lattice parameters indicated.

Table 1 Calculated lowest vibrational frequencies $\nu_{\min}$ (cm^{-1}), HOMO–LUMO energy gaps ΔE_{gap} (eV), and NICS (ppm) values at the geometrical centers of **1**–**8** and **10**

Cluster	Symmetry	$\nu_{\min}$ (cm^{-1})	ΔE_{gap} (eV)	NICS (ppm)
$B_{152}H_{84}$ (**1**)	T_h	133.5	4.37	−2.23
$B_{12}@B_{152}H_{72}{}^{2-}$ (**2**)	T_h	82.6	3.58	−17.79
$C_2B_{10}@B_{152}H_{72}$ (**3**)	C_{2h}	132.3	3.83	−20.25
$B_{12}@B_{144}H_{66}$ (**4**)	D_{3d}	86.21	2.85	−19.92
$C_{24}B_{120}H_{84}$ (**5**)	I_h	127.0	6.59	−3.51
$B_{12}@C_{24}B_{120}H_{72}{}^{2-}$ (**6**)	I_h	140.3	7.09	−27.22
$C_2B_{10}@C_{24}B_{120}H_{72}$ (**7**)	D_{5d}	141.7	6.04	−27.94
$B_{36}H_{32}{}^{2-}$ (**8**)	D_{2h}	50.50	6.07	−27.99
$B_{84}H_{60}{}^{2-}$ (**10**)	D_{3d}	67.53	4.91	−22.17

(which are even higher than the corresponding value (3.04 eV) of I_h C_{60} at the same theoretical level, except for $B_{12}@B_{144}H_{66}$ (**4**)) and negative calculated NICS values between NICS = −17.79–−35.30 ppm at the geometrical centers (Table 1), indicating that they are all spherically aromatic in nature and highly chemically stable.

It is also noticed that the core–shell superpolyhedral boranes and carboranes (**2**, **3**, **4**, **6**, and **7**) have significantly larger negative NICS values than their corresponding empty shells (1 and 5), indicating that both the closo-B_{12} and closo-C_2B_{10} cores help to improve the overall spherical aromaticity of the systems effectively.

The neutral T_h $B_{152}H_{84}$ (**1**) in Fig. 1 is assembled from twelve I_h $B_{12}H_{12}{}^{2-}$ icosahedra in the structural motif of C_{60} by releasing thirty H_2 molecules, with eight hexacoordinate B atoms in eight η^6-B_6 hexagons added on the cage surface to compensate for the 24 valence electrons deficiency of the system according to Wade's n+1 rule. The 1+12 core–shell suprapolyhedral borane T_h $B_{12}@B_{152}H_{72}{}^{2-}$ (**2**) is constructed by insertion of an icosahedral B_{12} core at the cage center of $B_{152}H_{84}$ (**1**) which is covalently satisfied by twelve inter-cage B–B σ single bonds (~ 1.63 Å) in radial directions with the twelve B_{12} icosahedral units evenly distributed on the cage surface in the first coordination sphere. The T_h $B_{12}{}^{2-}$ core at the center of the dianion (**2**) follows the Wade's n+1 rule with two extra electrons. Using a para-icosahedral 1,2-C_2B_{10} to replace the B_{12} core, the neutral 1+12 suprapolyhedral carborane C_{2h} $C_2B_{10}@B_{152}H_{72}$ (**3**) is generated.

Eliminating the eight hexacoordinate B atoms on the cage surface of $B_{12}@B_{152}H_{72}{}^{2-}$ (**2**) and six H atoms from the top and bottom while assigning six B–H–B 3c–2e bonds in a D_{3d} symmetry between neighboring B_{12} icosahedra on the waist generate the nearly close-packed core–shell D_{3d} $B_{12}@B_{144}H_{66}$ (4) which, as a true minimum of the neutral, contains a D_{3d} B_{12} core with six equivalent B–B 2c–2e σ bonds ($r_{\text{B–B}}$ = 1.69 Å) in vertical direction and six equivalent B–B–B 3c–2e bonds with six B_{12} icosahedrons around it on the waist. Encouragingly, the thus-obtained $B_{12}@B_{144}H_{66}$ (**4**) contains a D_{3d} B_{12} core which has exactly the same symmetry as the D_{3d} B_{12} unit cell in the experimentally known α-B_{12} (**12**) and possesses the same coordination environment with the twelve B_{12} icosahedra in the first coordination sphere as that of a D_{3d} B_{12} unit cell in α-B_{12} boron (**12**). $B_{12}@B_{144}H_{66}$ (**4**) can thus be viewed as the core–shell suprapolyhedral borane "seed" of 3D α-B_{12} (**12**) in a bottom-up approach by a periodic expansion in three dimensions via a complete dehydrogenation, as demonstrated in Fig. 2. $B_{12}@B_{144}H_{66}$ (**4**) is the first suprapolyhedral borane cluster reported to date which can serve as the "seed" of an experimentally known bulk boron allotrope in a bottom-up strategy.

As mentioned above, D_{5d} 1,12-$C_2B_{10}H_{12}$ can be used as building blocks to form the perfect cage-like superpolyhedral carborane I_h $C_{24}B_{120}H_{84}$ (**5**) (^1A_g) which can be expanded to the 1+12 core–shell superpolyhedral carborane I_h $B_{12}@C_{24}B_{120}H_{72}^{2-}$ (**6**) (^1A_g) with an icosahedral I_h B_{12} core at the center and D_{5d} $C_2B_{10}@C_{24}B_{120}H_{72}$ (**7**) (^1A_g) with an icosahedral D_{5d} C_2B_{10} core at the center, respectively. As shown in Table 1, with ν_{min} = 140.3, 141.7 cm^{-1}, ΔE_{gap} = 7.09, 6.04 eV, and NICS = −27.22, −27.94 ppm, respectively, both the 1+12 core–shell $B_{12}@C_{24}B_{120}H_{72}^{2-}$ (**6**) and $C_2B_{10}@C_{24}B_{120}H_{72}$ (**7**) as true minima of the systems are spherically aromatic and highly chemically stable. It is easy to understand that both the twelve C_2B_{10} icosahedra on the cage surface and the C_2B_{10} icosahedral core at the center in $C_2B_{10}@C_{24}B_{120}H_{72}$ (**7**) match the Wade's *n*+1 rule, while with two extra electrons, the icosahedral B_{12}^{2-} core in the dianionic $B_{12}@C_{24}B_{120}H_{72}^{2-}$ (**6**) also behaves like a superatom.

Following a similar superatom-assembling pattern, we designed the linear D_{2h} $B_{36}H_{32}^{2-}$ (**8**) in Fig. 2 which contains two B–H–B 3c–2e bonds between neighboring B_{12} units. The central $B_{12}H_{10}$ unit with four B–H–B 3c–2e bonds in 8 matches the Wade's *n*+1 rule due to the fact that the formation of one B–H–B 3c–2e bond contributes half a skeleton electron to the related B_{12} unit. It turns out to be true, as shown in the bonding analyses detailed in Fig. 4. Intriguingly, as shown in Fig. 2, the linear $B_{36}H_{32}^{2-}$ (**8**) can be extended periodically along the C_2 molecular axis to form the infinite 1D α-rhombohedral borane nanowire $B_{12}H_{10}$ (*Pmmm*) (**9**) with the calculated lattice parameter of *a* = 4.90 Å at GGA-PBE in which each $B_{12}H_{10}$ unit cell forms four B–H–B 3c–2e bonds with its two equivalent $B_{12}H_{10}$ neighbors. 1D $B_{12}H_{10}$ (**9**) as a true minimum of the system without imaginary phonon frequencies (Fig. 3(a)) can thus be viewed as a superatom-assembled mono-chain borane nanowire. It turns out to be a semiconductor in nature with the direct band gap of 5.54 eV at HSE06, as shown in its calculated band structures and projected densities of states (PDOS) depicted in Fig. 3.

The superatom-assembled close-packed perfect hexagonal D_{3d} $B_{84}H_{60}^{2-}$ (**10**) contains a D_{3d} $B_{12}H_6$ icosahedron at the center surrounded by six equivalent periphery $B_{12}H_9$ units around it. As highlighted in blue in Fig. 2, the central $B_{12}H_6$ unit forms six equivalent B–B–B 3c–2e bonds with its six periphery B_{12} icosahedral ligands on the mirror plane in a D_{3d} distribution. Such a hexagonal planar dianion can be extended in two dimensions to form the perfect 2D α-rhombohedral monolayer borophane $B_{12}H_6$ ($P\bar{3}m1$) (**11**) without imaginary phonon frequencies (Fig. 3(b)) which, as a semiconductor with the calculated indirect bond gap of 2.25 eV at HSE06, is a close-packed 2D self-assembled monolayer (SAM) borophane with the optimized lattice parameters of *a* = *b* = 4.87 Å, and *γ* = 120° at GGA-PBE (Fig. 3). We also notice that the D_{3d} $B_{12}H_6$ core in the close-packed $B_{84}H_{60}^{2-}$

(a) 1D $B_{12}H_{10}$ (**9**)

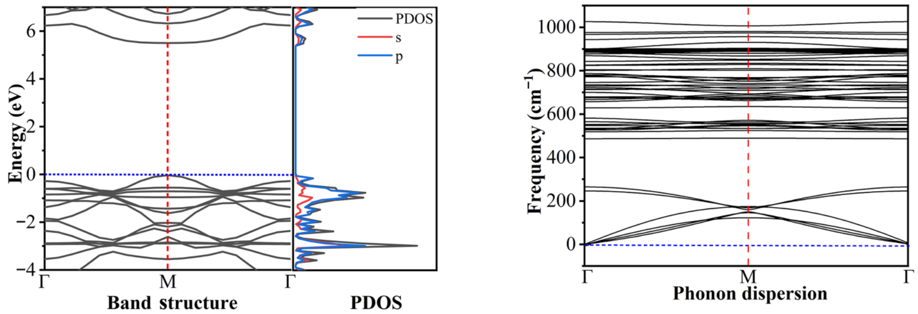

(b) 2D $B_{12}H_6$ (**11**)

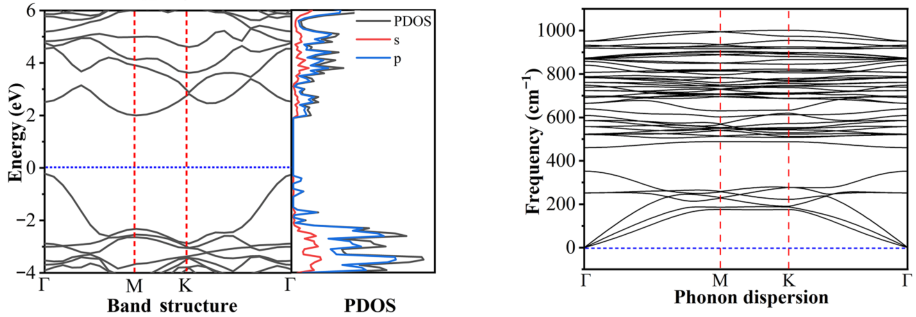

(c) 3D α-B_{12} (**12**)

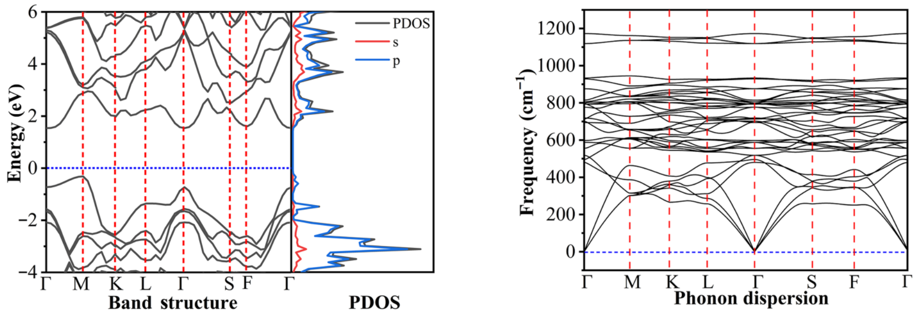

Figure 3 Calculated band structures and PDOS, and phonon dispersion spectra of (a) 1D $B_{12}H_{10}$ (**9**), (b) 2D $B_{12}H_6$ (**11**), and (c) 3D α-B_{12} (**12**) at the hybrid HSE06 level.

(**10**) can be removed from the dianion to form a perfect hexagonal ring D_{3d} $B_{72}H_{60}$ (**13**) which is a true minimum of the system analogous to benzene (Fig. S2 in the ESM).

More profoundly, the core–shell D_{3d} $B_{12}@B_{144}H_{66}$ (**4**) can be expanded in three dimensions in a bottom-up approach via a complete dehydrogenation to form the experimentally known nearly close-packed 3D α-B_{12} ($R\bar{3}m$) (**12**) without imaginary phonon frequencies (Fig. 3(c)) which can also be viewed as an assembly of the monolayer $B_{12}H_6$ (**11**) staggered in vertical direction. With the optimized lattice parameters of $a = b = c =$ 5.01 Å and $\alpha = \beta = \gamma = 57.99°$ at GGA-PBE (Fig. 2) and indirect band gap of 1.85 eV at HSE06 (close to the experimental value of 2.0 eV [44]) (Fig. 3), 3D α-B_{12} (**12**) has the calculated B–B bond lengths of $r_{\text{B–B}}$ = 1.66 Å between the B_{12} unit cell and its six B_{12} icosahedral neighbors on the vertical direction and the B–B distances of $r_{\text{B–B}}$ = 1.98 Å with its six B_{12} icosahedral B_{12} neighbors in the horizontal plane where each D_{3d} B_{12} unit cell forms six equivalent B–B–B 3c–2e σ-bonds with its six D_{3d} B_{12} neighbors. Thus, as outlined in Fig. 2, starting from a perfect icosahedral I_h $B_{12}H_{12}^{2-}$, the 1D mono-chain nanowire $B_{12}H_{10}$ (**9**), 2D SAM $B_{12}H_6$ (**11**), and 3D α-B_{12} (**12**) can be systematically assembled in a bottom-up approach via partial or complete dehydrogenations.

Extensive Born–Oppenheimer molecular dynamics (BOMD) simulations on $B_{12}@B_{152}H_{72}^{2-}$ (**2**) at 500K, $B_{12}@B_{144}H_{66}$ (**4**) at 1000 K, and $C_2B_{10}@C_{24}B_{120}H_{72}$ (**7**) at 1200 K in Fig. S3 in the ESM clearly indicate that these core–shell suprapolyhedral species are all highly dynamically stable, as evidenced by their small calculated average root-mean-square-deviations of RMSD = 0.08/0.10/0.09 Å and maximum bond length deviations of MAXD = 0.63/0.39/0.40 Å, respectively. These core–shell structures are all well maintained during BOMD simulations in 30 ps, with no low-lying isomers observed. We also assess the dynamic stability of 1D $B_{12}H_{10}$ (**9**) at 800 K and 2D $B_{12}H_6$ (**11**) at 1000 K by performing BOMD simulations on a 1 × 1 × 4 and 4 × 4 × 1 supercell for 30 ps (Fig. S3 in the ESM). With the calculated RMSD = 0.09/0.10 Å and MAXD = 0.31/0.39 Å, respectively, these semiconducting crystals all appear to be highly dynamically stable at high temperatures.

3.2 Bonding pattern analyses

Detailed AdNDP and SSAdNDP bonding analyses unveil both the localized and delocalized bonds in the concerned zero-dimensional (0D), 1D, 2D, and 3D species [40, 41] and help to comprehend the bottom-up approach employed in this work. The spherically aromatic icosahedral I_h $B_{12}H_{12}^{2-}$ and D_{5d} $C_2B_{10}H_{12}$ with the superatomic electronic configuration of $1S^21P^61D^{10}1F^8$ are well-known to follow the Wade's n+1 rule (Fig. S1 in the ESM). Interestingly, as can be seen from Figs. 4(a) and 4(d), both the central D_{2h} $B_{12}H_{10}$ unit in $B_{36}H_{32}^{2-}$ (**8**) and D_{2h} $B_{12}H_{10}$ unit cell in 1D nanowire $B_{12}H_{10}$ (**9**) possess 1 S-type bond, 3 P-type bonds, 5 D-type bonds, and 4 F-type bonds following the superatomic skeleton electronic configuration of $1S^21P^61D^{10}1F^8$. Similarly, the central D_{3d} $B_{12}H_6$ unit in $B_{84}H_{60}^{2-}$ (**10**) and D_{3d} $B_{12}H_6$ unit cell in 2D borophane $B_{12}H_6$ (**11**) contain 1 S-type bond, 3 P-type bonds, 5 D-type bonds, and 4 F-type skeleton bonds too, again matching the superatomic bonding pattern (Figs. 4(b) and 4(e)). More intriguingly, as demonstrated in Figs. 4(c) and 4(f), in addition to the 6 equivalent B–B 2c–2e σ bonds with six B_{12} icosahedra in vertical direction and 6 equivalent B–B–B 3c–2e bonds with six B_{12} icosahedra on the waist, both the central D_{3d} B_{12} unit in $B_{12}@B_{144}H_{66}$ (**4**) and D_{3d} B_{12} unit cell in 3D α-B_{12} (**12**) also possess 1 S-type bond, 3 P-type bonds, 5 D-type bonds, and 4 F-type skeleton bonds, again matching the Wade's rule. The 0D, 1D, 2D, and 3D species in Figs. 1 and 2 can thus all be viewed as low-dimensional nanostructures assembled in bottom-up approaches

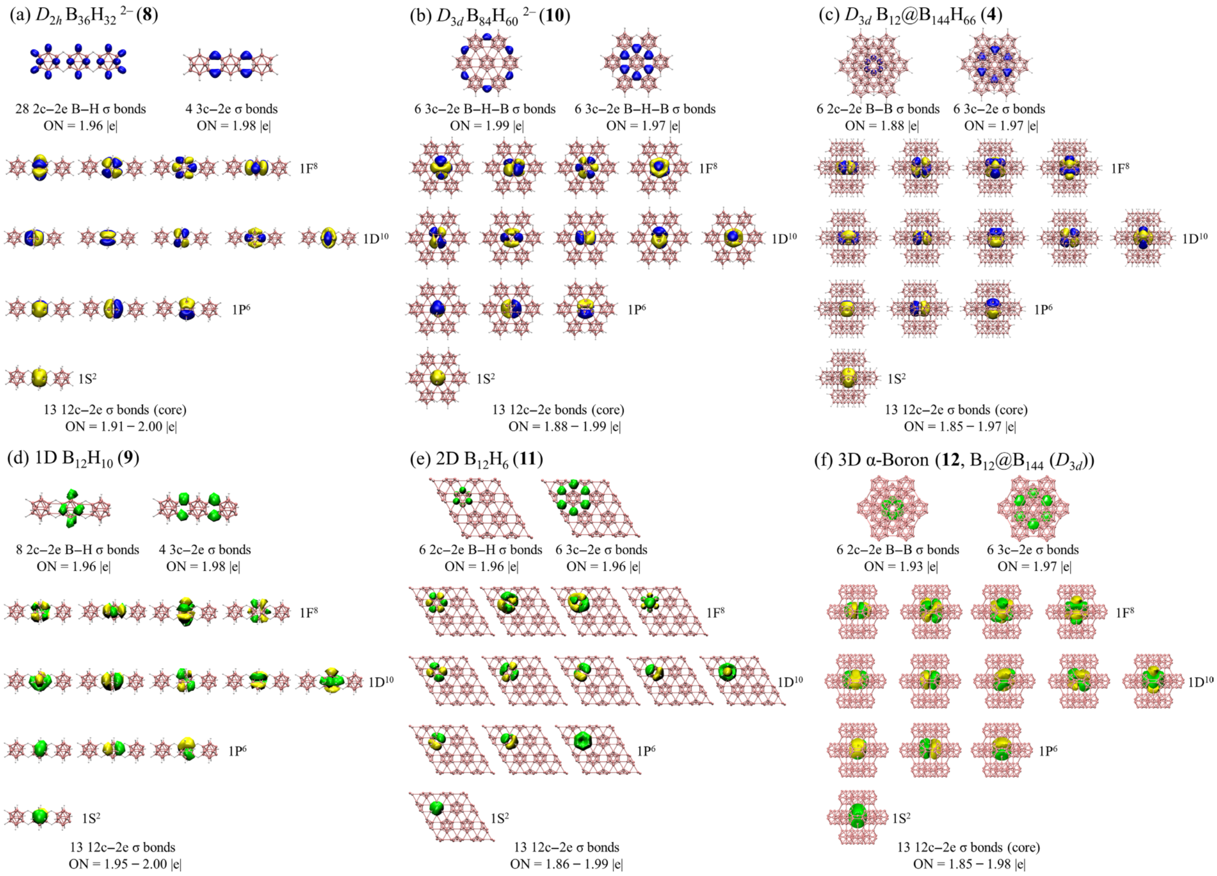

Figure 4 Comparison of the AdNDP bonding patterns of (a) D_{2h} $B_{36}H_{32}^{2-}$ (**8**), (b) D_{3d} $B_{84}H_{60}^{2-}$ (**10**), (c) D_{3d} $B_{12}@B_{144}H_{66}$ (**4**), (d) 1D $B_{12}H_{10}$ (**9**), (e) 2D $B_{12}H_6$ (**11**), and (f) 3D α-rhombohedral boron (**12**). For brevity, only the chemical bonds related to the central B_{12} units in $B_{36}H_{32}^{2-}$ (**8**), $B_{84}H_{60}^{2-}$ (**10**), and $B_{12}@B_{144}H_{66}$ (**4**) are depicted here, with their complete bonding patterns presented in Fig. S4 in the ESM.

based on the spherically aromatic icosahedral B_{12} and C_2B_{10} units which possess the universal superatomic skeleton electronic configuration of $1S^21P^61D^{10}1F^8$.

The calculated NICS-ZZ distributions depicted in Fig. 5 further evidence the superatomic aromatic nature of the icosahedral B_{12} and C_2B_{10} units in D_{2h} $B_{36}H_{32}^{2-}$ (**8**), D_{3d} $B_{84}H_{60}^{2-}$ (**10**), D_{3d} $B_{12}@B_{144}H_{66}$ (**4**), and D_{5d} $C_2B_{10}@C_{24}B_{120}H_{72}$ (**7**) where the NICS-ZZ value at the center of each B_{12} or C_2B_{10} icosahedron is highly negative. Similar negative NICS-ZZ distributions are expected to exist in 1D $B_{12}H_{10}$ (**9**), 2D $B_{12}H_6$ (**11**), and 3D α-B_{12} (**12**) where each icosahedral B_{12} unit cell follows the skeleton electronic configuration of $1S^21P^61D^{10}1F^8$ and matches the Wade's n+1 rule, as demonstrated in details in Figs. 4(d)–4(f), respectively.

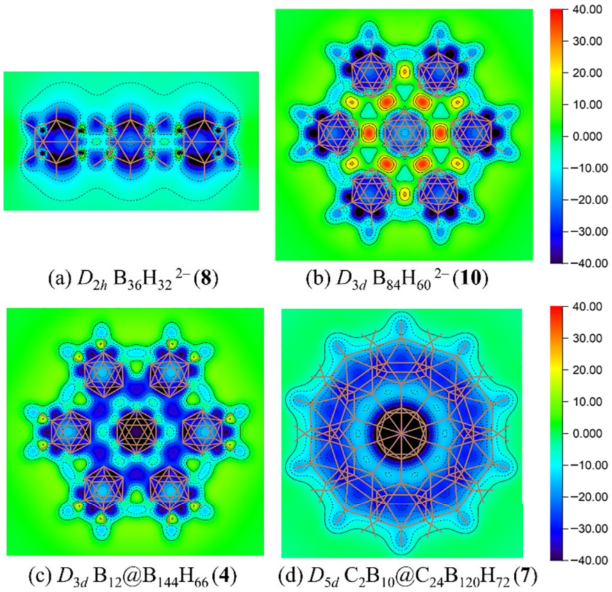

(a) D_{2h} $B_{36}H_{32}{}^{2-}$ (**8**) (b) D_{3d} $B_{84}H_{60}{}^{2-}$ (**10**)

(c) D_{3d} $B_{12}@B_{144}H_{66}$ (**4**) (d) D_{5d} $C_2B_{10}@C_{24}B_{120}H_{72}$ (**7**)

Figure 5 NICS-ZZ distributions of (a) D_{2h} $B_{36}H_{32}^{2-}$ (**8**), (b) D_{3d} $B_{84}H_{60}^{2-}$ (**10**), (c) D_{3d} $B_{12}@B_{144}H_{66}$ (**4**), and (d) D_{5d} $C_2B_{10}@C_{24}B_{120}H_{72}$ (**7**) at PBE0/6-31G(d) level.

3.3 Spectral simulations

The IR and Raman spectra of the most-concerned neutral core–shell superpolyhedral borane and carborane were computationally simulated in Fig. 6 to facilitate their future experimental characterizations. D_{3d} $B_{12}@B_{144}H_{66}$ (**4**) exhibits two strong IR absorptions at 1890 cm^{-1} (a_g) and 2706 cm^{-1} (a_g) and three Raman active peaks at 211 cm^{-1} (a_g), 2707 cm^{-1} (a_g), and 2765 cm^{-1} (a_g), with a 183 cm^{-1} (a_g) symmetrical vibration corresponding to typical radial breathing modes (RBMs) of the system. The major IR active peak of D_{5d} $C_2B_{10}@C_{24}B_{120}H_{72}$ (**7**) occurs at 2735 cm^{-1} (e_{1u}). The four vibration modes at 207 cm^{-1} (a_{1g}), 253 cm^{-1} (a_{1g}), 2774 cm^{-1} (a_{1g}), and 3276 cm^{-1} (a_{1g}) could be used as Raman fingerprints to characterize the D_{5d} species. The strong Raman peaks 253 cm^{-1} (a_g) represents its typical RBM.

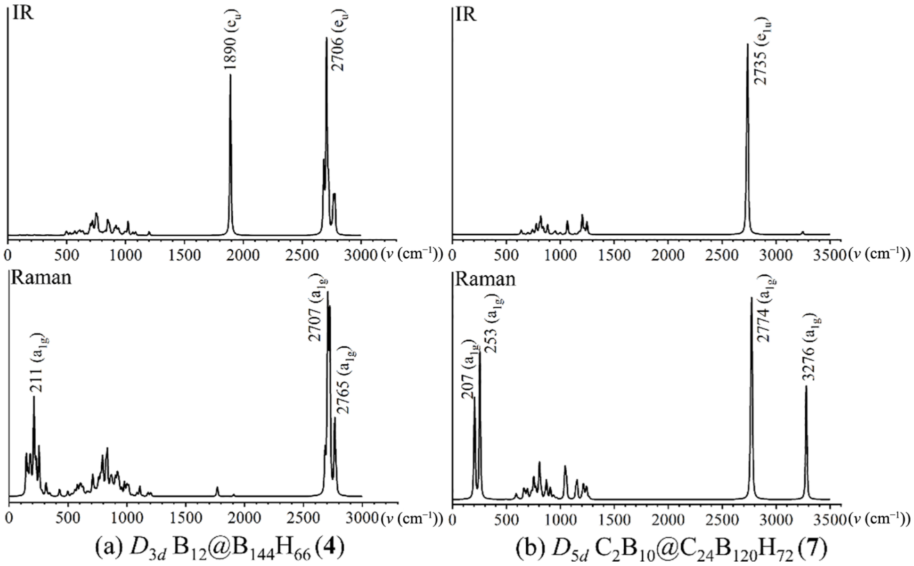

(a) D_{3d} $B_{12}@B_{144}H_{66}$ (**4**) (b) D_{5d} $C_2B_{10}@C_{24}B_{120}H_{72}$ (**7**)

Figure 6 Simulated IR and Raman spectra of (a) D_{3d} $B_{12}@B_{144}H_{66}$ (**4**) and (b) D_{5d} $C_2B_{10}@C_{24}B_{120}H_{72}$ (**7**) at PBE0/6-31G(d) level.

4 Conclusions

In summary, a series of superatom-assembled boranes and carboranes T_h $B_{12}@B_{152}H_{72}^{2-}$ (**2**), C_{2h} $C_2B_{10}@B_{152}H_{72}$ (**3**), D_{3d} $B_{12}@B_{144}H_{66}$ (**4**), I_h $B_{12}@C_{24}B_{120}H_{72}^{2-}$ (**6**), D_{5d} $C_2B_{10}@C_{24}B_{120}H_{72}$ (**7**), D_{2h} $B_{36}H_{32}^{2-}$ (**8**), and D_{3d} $B_{84}H_{60}^{2-}$ (**10**) have been predicted at DFT in this work which can be extended to form the 1D borane nanowire $B_{12}H_{10}$ (**9**), 2D monolayer borophane $B_{12}H_6$ (**11**), and 3D α-B_{12} (**12**) boron semiconductors via partial or complete dehydrogenizations. Detailed bonding analyses indicate that the high stability of these superatom-assembled nanostructures can be traced back to the spherical aromaticity of their icosahedral B_{12} or C_2B_{10} structural units which follow the Wade's n+1 rule in skeleton electron counts. Similar to graphene, the monolayer $B_{12}H_6$ (**11**) could be rolled into 1D α-rhombohedral borane nanotubes or assembled into 2D few-layered α-rhombohedral borophanes staggered in vertical direction. Such superatom-assembled nano-structures based on icosahedral closo-B_{12} and closo-C_2B_{10} are expected to be realized in future experiments to extend the structural domain of boron-based nanomaterials.

Acknowledgements

This work was supported by the National Natural Science Foundation of China (Nos. 22373061, 21973057, and 22003034).

Electronic Supplementary Material: Supplementary material (superatomic structures and their bonding patterns, molecular dynamical simulations, AdNDP bonding analyses, and optimized coordinates) is available in the online version of this article at https://doi.org/10.1007/s12274-024-6609-2.

References

[1] Reber, A. C.; Khanna, S. N.; Castleman, A. W. Superatom compounds, clusters, and assemblies: Ultra alkali motifs and

architectures. *J. Am. Chem. Soc.* **2007**, *129*, 10189–10194.

[2] Castleman, A. W. Jr.; Khanna, S. N. Clusters, superatoms, and building blocks of new materials. *J. Phys. Chem. C* **2009**, *113*, 2664–2675.

[3] Aikens, C. M. Electronic structure of ligand-passivated gold and silver nanoclusters. *J. Phys. Chem. Lett.* **2011**, *2*, 99–104.

[4] Jia, Y. H.; Luo, Z. X. Thirteen-atom metal clusters for genetic materials. *Coordinat. Chem. Rev.* **2019**, *400*, 213053.

[5] Cotton, F. A.; Wilkinson, G.; Murillo, C. A.; Bochmann, M. *Advanced Inorganic Chemistry, Wiley-Interscience*, 6th ed. Wiley: New York, 1999.

[6] Hosmane, N. S. *Boron Science: New Technologies and Applications*; CRC Press: Boca Raton, 2011.

[7] Grimes, R. N. *Carboranes*, 3rd ed. Elsevier: Oxford, 2016.

[8] Sivaev, I. B.; Bregadze, V. I.; Sjöberg, S. Chemistry of *closo*-dodecaborate anion $[B_{12}H_{12}]^{2-}$: A review. *Collect. Czech. Chem. Commun.* **2002**, *67*, 679–727.

[9] Sivaev, I. B.; Stogniy, M. Y. Mercury derivatives of polyhedral boranes, carboranes, and metallacarboranes. *Russ. Chem. Bull.* **2019**, *68*, 217–253.

[10] Chen, H.; Qiu, Y. Q.; Sun, S. L.; Liu, C. G.; Su, Z. M. Density functional theory study on the structures and stabilities of 14-vertex *closo*-carborane isomers. *Acta Chim. Sin.* **2007**, *65*, 305–309.

[11] Wade, K. The structural significance of the number of skeletal bonding electron-pairs in carboranes, the higher boranes and borane anions, and various transition-metal carbonyl cluster compounds. *J. Chem. Soc. D* **1971**, 792–793

[12] Oganov, A. R.; Chen, J. H.; Gatti, C.; Ma, Y. Z.; Ma, Y. M.; Glass, C. W.; Liu, Z. X.; Yu, T.; Kurakevych, O. O.; Solozhenko, V. L. Ionic high-pressure form of elemental boron. *Nature* **2009**, *457*, 863–867.

[13] Albert, B.; Hillebrecht, H. Boron: Elementary challenge for experimenters and theoreticians. *Angew. Chem., Int. Ed.* **2009**, *48*, 8640–8668.

[14] McCarty, L. V.; Kasper, J. S.; Horn, F. H.; Decker, B. F.; Newkirk, A. E. A new crystalline modification of boron. *J. Am. Chem. Soc.* **1958**, *80*, 2592.

[15] Tai, G. A.; Hu, T. S.; Zhou, Y. G.; Wang, X. F.; Kong, J. Z.; Zeng, T.; You, Y. C.; Wang, Q. Synthesis of atomically thin boron films on copper foils. *Angew. Chem., Int. Ed.* **2015**, *54*, 15473–15477.

[16] Zubarev, D. Y.; Boldyrev, A. I. Comprehensive analysis of chemical bonding in boron clusters. *J. Comput. Chem.* **2007**, *28*, 251–268.

[17] Huang, W.; Sergeeva, A. P.; Zhai, H. J.; Averkiev, B. B.; Wang, L. S.; Boldyrev, A. I. A concentric planar doubly π-aromatic B_{19}^{-} cluster. *Nat. Chem.* **2010**, *2*, 202–206.

[18] Sergeeva, A. P.; Averkiev, B.; Zhai, H. J.; Boldyrev, A. I.; Wang, L. S. All-boron analogues of aromatic hydrocarbons: B_{17}^{-} and B_{18}^{-}. *J. Chem. Phys.* **2011**, *134*, 224304.

[19] Romanescu, C.; Harding, D. J.; Fielicke, A.; Wang, L. S. Probing the structures of neutral boron clusters using infrared/vacuum ultraviolet two color ionization: B_{11}, B_{16}, and B_{17}. *J. Chem. Phys.* **2012**, *137*, 014317.

[20] Jalife, S.; Liu, L.; Pan, S.; Cabellos, J. L.; Osorio, E.; Lu, C.; Heine, T.; Donald, K. J.; Merino, G. Dynamical behavior of boron clusters. *Nanoscale* **2016**, *8*, 17639–17644.

[21] Wang, L. S. Photoelectron spectroscopy of size-selected boron clusters: From planar structures to borophenes and borospherenes. *Int. Rev. Phys. Chem.* **2016**, *35*, 69–142.

[22] Jian, T.; Chen, X. N.; Li, S. D.; Boldyrev, A. I.; Li, J.; Wang, L. S. Probing the structures and bonding of size-selected boron and doped-boron clusters. *Chem. Soc. Rev.* **2019**, *48*, 3550–3591.

[23] Wang, Y. J.; Zhao, Y. F.; Li, W. L.; Jian, T.; Chen, Q.; You, X. R.; Ou, T.; Zhao, X. Y.; Zhai, H. J.; Li, S. D.; Wang, L. S. Observation and characterization of the smallest borospherene, B_{28} and B_{28}^{-}. *J. Chem. Phys.* **2016**, *144*, 064307.

[24] Chen, Q.; Li, W. L.; Zhao, Y. F.; Zhang, S. Y.; Hu, H. S.; Bai, H.; Li, H. R.; Tian, W. J.; Lu, H. G.; Zhai, H. J. et al. Experimental and theoretical evidence of an axially chiral borospherene. *ACS nano* **2015**, *9*, 754–760.

[25] Zhai, H. J.; Zhao, Y. F.; Li, W. L.; Chen, Q.; Bai, H.; Hu, H. S.; Piazza, Z. A.; Tian, W. J.; Lu, H. G.; Wu, Y. B. Observation of an all-boron fullerene. *Nat. Chem.* **2014**, *6*, 727–731.

[26] Chen, W. J.; Ma, Y. Y.; Chen, T. T.; Ao, M. Z.; Yuan, D. F.; Chen, Q.; Tian, X. X.; Mu, Y. W.; Li, S. D.; Wang, L. S. B_{48}^{-}: A bilayer boron cluster. *Nanoscale* **2021**, *13*, 3868–3876

[27] Adamo, C.; Barone, V. Toward reliable density functional methods without adjustable parameters: The PBE0 model. *J. Chem. Phys.* **1999**, *110*, 6158–6170.

[28] Becke, A. D. Density-functional thermochemistry. I. The effect of the exchange-only gradient correction. *J. Chem. Phys.* **1992**, *96*, 2155–2160.

[29] Bhattacharya, D.; Klein, D. J.; Oliva, J. M.; Griffin, L. L.; Alcoba, D. R.; Massaccesi, G. E. Icosahedral symmetry super-carborane and beyond. *Chem. Phys. Lett.* **2014**, *616*, 16–19.

[30] Klod, S.; Kleinpeter, E. *Ab initio* calculation of the anisotropy effect of multiple bonds and the ring current effect of arenes—Application in conformational and configurational analysis. *J. Chem. Soc. Perkin Trans.* **2001**, *2*, 1893–1898.

[31] Kleinpeter, E.; Klod, S.; Koch, A. Visualization of through space NMR shieldings of aromatic and anti-aromatic molecules and a simple means to compare and estimate aromaticity. *J. Mol. Struct. THEOCHEM* **2007**, *811*, 45–60.

[32] Lu, T.; Chen, F. W. Multiwfn: A multifunctional wavefunction analyzer. *J. Comput. Chem.* **2012**, *33*, 580–592.

[33] Kresse, G.; Furthmüller, J. Efficiency of *ab-initio* total energy calculations for metals and semiconductors using a plane-wave basis set. *Comput. Mater. Sci.* **1996**, *6*, 15–50.

[34] Kresse, G.; Furthmüller, J. Efficient iterative schemes for *ab initio* total-energy calculations using a plane-wave basis set. *Phys. Rev. B* **1996**, *54*, 11169–11186.

[35] Perdew, J. P.; Burke, K.; Ernzerhof, M. Generalized gradient approximation made simple. *Phys. Rev. Lett.* **1996**, *77*, 3865–3868.

[36] Monkhorst, H. J.; Pack, J. D. Special points for Brillouin-zone integrations. *Phys. Rev. B* **1976**, *13*, 5188–5192.

[37] Togo, A.; Oba, F.; Tanaka, I. First-principles calculations of the ferroelastic transition between rutile-type and $CaCl_2$-type SiO_2 at high pressures. *Phys. Rev. B* **2008**, *78*, 134106.

[38] Heyd, J.; Scuseria, G. E.; Ernzerhof, M. Hybrid functionals based on a screened Coulomb potential. *J. Chem. Phys.* **2003**, *118*, 8207–8215.

[39] VandeVondele, J.; Krack, M.; Mohamed, F.; Parrinello, M.; Chassaing, T.; Hutter, J. Quickstep: Fast and accurate density functional calculations using a mixed Gaussian and plane waves approach. *Comput. Phys. Commun.* **2005**, *167*, 103–128.

[40] Zubarev, D. Y.; Boldyrev, A. I. Developing paradigms of chemical bonding: Adaptive natural density partitioning. *Phys. Chem. Chem. Phys.* **2008**, *10*, 5207–5217.

[41] Galeev, T. R.; Dunnington, B. D.; Schmidt, J. R.; Boldyrev, A. I. Solid state adaptive natural density partitioning: A tool for deciphering multi-center bonding in periodic systems. *Phys. Chem. Chem. Phys.* **2013**, *15*, 5022–5029.

[42] Humphrey, W.; Dalke, A.; Schulten, K. VMD: Visual molecular dynamics. *J. Mol. Graph.* **1996**, *14*, 33–38.

[43] Frisch, M. J.; Trucks, G. W.; Schlegel, H. B.; Scuseria, G. E.; Robb, M. A.; Cheeseman, J. R.; Scalmani, G.; Barone, V.; Petersson, G. A.; Nakatsuji, H. et al. *Gaussian 16* (*Revision B. 01*); Gaussian, Inc.: Wallingford, 2016.

[44] Hubbard, F. H. Some electrical and optical properties of simple rhombohedral boron. *J. Appl. Phys.* **1959**, *30*, 1611–1612.